ELSEVIER

Journal of Fluids and Structures 19 (2004) 291–306

JOURNAL OF FLUIDS AND STRUCTURES

www.elsevier.nl/locate/jnlabr/yjfls

Effects of geometric structural nonlinearity on flutter and limit cycle oscillations of high-aspect-ratio wings

D.M. Tang, E.H. Dowell*

Department of Mechanical Engineering and Materials Science, Duke University, Box 90300, Durham, NC 27708-0300, USA

Received 24 July 2000; accepted 12 October 2003

Abstract

In this paper structural equations of motion based on nonlinear beam theory and the ONERA aerodynamic stall model are used to study the effects of geometric structural nonlinearity on flutter and limit cycle oscillations (LCO) of high-aspect-ratio wings. For example, the effects of large static pre-flutter deformations in the vertical or torsional direction are considered. In particular, static deformations in the vertical and torsional directions caused by a static angle of attack, gravity and/or manufactured curvature generally decrease system stiffness and flutter stability. The structural nonlinearity also leads to a sensitivity to initial conditions as well as any parameter that influences the static equilibrium condition. A dynamic perturbation equation about a nonlinear static equilibrium is derived which is used to determine the small perturbation flutter boundary. The effects of the geometric structural nonlinearity of the beam theory on both the perturbation flutter boundary and the nonlinear response are significant. Onset of a limit cycle oscillation is dependent upon the delicate between stall aerodynamics and structural nonlinear forces. LCO above and below the perturbation flutter boundary generally occurs over a limited range of flow velocity. LCO can occur below the perturbation flutter velocity due to large initial disturbances.

1. Introduction

Linear and nonlinear aeroelastic stability and response of an aircraft with a high-aspect-ratio wing have been studied for many years from subsonic to supersonic flow. Most investigators have used linear beam theory to simplify the wing structural model. As shown in Hodges and Dowell (1974) and Patil et al. (1999a), however a geometric structural nonlinearity may arise from the coupling between elastic flap bending, chordwise bending and torsion.

For low-aspect-ratio wings nonlinear plate theory has been used as a wing structural model by Tang et al. (1999a). As is well known, Von Karman's plate equations take into account the nonlinear coupling between in–plane and out-of-plane plate motion as a result of retaining quadratic terms in the strain–displacement equations. Physically, there is a stiffening of the plate due to an in-plane tension which increases quadratically with increasing out-of-plane displacement. This geometric structural nonlinear coupling leads to a limit cycle oscillation (LCO) when the flow velocity *exceeds* the linear small perturbation flutter speed of this system. The contribution of this structural nonlinear coupling to aeroelastic stability and response is beneficial. Theoretical and experimental results are shown by Tang et al.(1999a,b) to be in good agreement for low-aspect-ratio wing models in low subsonic flow.

In this paper we use structural equations of motion based on nonlinear beam theory, see Hodges and Dowell (1974) and the original ONERA aerodynamic stall model by Tran and Petot (1981) to study the effects of geometric structural

*Corresponding author. Tel.: +1-919-660-5302; fax: +1-919-660-0089.
E-mail address: dowell@ee.duke.edu (E.H. Dowell).

0889-9746/$ - see front matter © 2004 Elsevier Ltd. All rights reserved.
doi:10.1016/j.jfluidstructs.2003.10.007

Nomenclature

$c, \bar{c}$	wing chord and dimensionless chord, c/L
C_l	section lift coefficient
C_d	section drag coefficient
C_m	section torsional moment coefficient
$\mathrm{d}D, dL$	section drag and lift forces
$\mathrm{d}M_0$	section pitch moment about 1/4 chord
$\mathrm{d}F_v, \mathrm{d}F_w$	section chordwise and vertical component forces
$\mathrm{d}M_x$	section pitch moment about elastic axis
E	modulus of elasticity
g	gravitational constant
G	shear modulus
I_1, I_2	vertical, chordwise area moments
J	torsional stiffness constant
K_m	wing mass radius of gyration
L	wing span
m	mass per unit length of the wing
M	tip mass of the wing
N	total number of modes
NN	number of aerodynamic elements
t	time
U	free stream velocity
v	chordwise bending deflection
w	vertical bending deflection, perpendicular to v
V_j, W_j	generalized coordinates for bending
W_{tip}	tip displacement due to manufactured curvature
x	position coordinate along wing span
y_{ac}	aerodynamic center of section from elastic axis
α_l	wing section angle of attack
β	$\equiv EI_2/EI_1 - 1$
Δ_l	dimensionless width of lth aerodynamic section
θ_0	steady angle of attack
λ	$\equiv \frac{1}{2}\rho U^2 \bar{c}\tau^2/m = \frac{1}{2}\rho U^2 \bar{c} L^4/EI_1$
μ	$\equiv M/mL$
ρ	air density
τ	characteristic time scale, $\sqrt{mL^4/EI_1}$
ϕ	twist about deformed elastic axis
Φ_j	generalized coordinates for torsion
$\omega_{\phi j}$	jth torsional natural frequency of wing
ω_{vj}	jth chordwise natural frequency of wing
ω_{wj}	jth vertical natural frequency of wing
$(\,)'$	$\mathrm{d}(\,)/\mathrm{d}x$
$(\dot{\cdot})$	$\mathrm{d}(\,)/\mathrm{d}t$

nonlinearity on flutter of high-aspect-ratio wings. Large static pre-flutter deformations in the vertical or torsional direction are considered. The large static deformation is created by one of several physical effects:

(i) a tip mass with inertia and gravity effects—Case 1;
(ii) a gravity tip force only due to tip mass (i.e., the inertia of the tip mass is neglected)—Case 2;
(iii) a manufactured curvature in the vertical direction—Case 3;
(iv) a steady angle of attack which creates a static aerodynamic load on the wing—Case 4.

A dynamic perturbation equation about a nonlinear static equilibrium is derived which is used to determine the flutter boundary. A direct time marching solution is also used to calculate the response behavior of this nonlinear

system above and below the nominal, perturbation flutter boundary. The results provide additional insight with respect to the contribution of structural nonlinear coupling to the aeroelastic stability and response of high-aspect-ratio wings. As such, this paper is a complement to the studies reported earlier by Patil et al. (1999a,b).

2. Nonlinear and perturbation flutter equations

A wing model with the parameters presented by Patil et al. (1999a) is used. See Table 1. However we use a simpler nonlinear beam theory in the present paper compared to that of Patil et al. (1999b). According to the Hodges–Dowell equations, for an uniform, untwisted elastic wing, neglecting cross-section warping, the equations of motion may be written as

$$EI_2 v'''' + (EI_2 - EI_1)(\phi(w + w_0)')' + m\ddot{v} + M\ddot{v}_{x=L} = \frac{\mathrm{d}F_v}{\mathrm{d}x}, \tag{1}$$

$$EI_1(w + w_0)'''' + (EI_2 - EI_1)(\phi v')' + m\ddot{w} + M\ddot{w}_{x=L} - Mg\delta(x - L) = \frac{\mathrm{d}F_w}{\mathrm{d}x}, \tag{2}$$

$$-GJ\phi'' + (EI_2 - EI_1)(w + w_0)' v'' + mK_m^2\ddot{\phi} = \frac{\mathrm{d}M_x}{\mathrm{d}x}. \tag{3}$$

A few general comments about Eqs. (1)–(3) may be in order. First of all by multiplying each of these equations by $\delta v, \delta w$ and $\delta\phi$, respectively, and integrating over the length of the beam, a variational statement may be derived. Conversely as shown in Hodges and Dowell (1974), these equations may be derived from Hamilton's principle.

Another interesting aspect of these equations is that using a method previously developed by Dowell (1969, 1970) and independently by Bejan (1984), order of magnitude analytical estimates may be derived for estimating under what conditions nonlinear effects may be important. A discussion of these estimates and their derivation is given in the appendix. This method may be used for a wide range of interesting nonlinear dynamical systems.

Note that in Eqs. (1)–(3) only the most important nonlinear terms are retained from the Hodges–Dowell equations and the third and higher order geometrically nonlinear terms are neglected here. Also note that the geometric twist angle $\hat{\phi} = \phi + \int_0^x v' w'' \mathrm{d}x$ is considered in the aerodynamic terms. M is the tip mass and w_0 is the manufactured curvature.

The v and w components of the aerodynamic force, and the aerodynamic moment about the elastic axis can be expressed as follows:

$$\begin{aligned} \mathrm{d}F_w &= \mathrm{d}L - (\phi_{\lambda} - \theta_0)\,\mathrm{d}D, \\ \mathrm{d}F_v &= -\mathrm{d}D - (\phi_{\lambda} - \theta_0)\,\mathrm{d}L, \\ \mathrm{d}M_x &= \mathrm{d}M_0 - y_{ac}\,\mathrm{d}F_w, \end{aligned} \tag{4}$$

Table 1
Wing model data

Wing	
Half-span	16 m
Chord	1 m
Mass per unit length	0.75 kg/m
Moment of Inertia (50% chord)	0.1 kg/m
Spanwise elastic axis	50% chord
Center of gravity	50% chord
Flap bending rigidity (EI_1)	2×10^4 N m^2
Chordwise bending rigidity (EI_2)	4×10^6 N m^2
Torsional rigidity (GJ)	1×10^4 N m^2
Flight conditions	
Altitude	20 km
Density of air	0.0889 kg/m^3

where

$$dL = \tfrac{1}{2}\rho c U^2 C_l\, dx, \quad dD = \tfrac{1}{2}\rho c U^2 C_d\, dx, \quad dM_0 = \tfrac{1}{2}\rho c^2 U^2 C_m\, dx,$$

$$\phi_\lambda \approx \dot{w}/(U + \dot{v} + \dot{w}\theta_0), \quad \alpha = \hat{\phi} + \theta_0 - \phi_\lambda,$$

where θ_0 is a steady angle of attack.

The section aerodynamic coefficients C_l, C_d and C_m are obtained from the original ONERA stall aerodynamic model, see Tran and Petot (1981).

From Eqs. (1)–(3), expansions in general mode shape functions are used to obtain ordinary differential equations in terms of generalized coordinates. They are expressed in series form as follows:

$$\bar{v} = \sum_{j=1}^{N} V_j(t)\psi_j(\bar{x}),$$

$$\bar{w} = \sum_{j=1}^{N} W_j(t)\psi_j(\bar{x}), \tag{5}$$

$$\phi = \sum_{j=1}^{N} \Phi_j(t)\Theta_j(\bar{x}),$$

where the over-bar indicates nondimensionalization with respect to the wing span, L, and ψ_j, Θ_j are the jth normal modes of the associated linear structural model.

Using the Galerkin method one obtains a set of nondimensional modal equations from Eqs. (1)–(5),

$$\sum_{j=1}^{N}\left[\delta_{ij}(\ddot{V}_j + \bar{\omega}_{vj}^2 V_j) + \mu D_{ij}\ddot{V}_j + \beta\sum_{k=1}^{N} K_{jki}\Phi_j W_k + \beta\bar{W}_{\text{tip}} S_{ij}\Phi_j\right]$$
$$= -p\sum_{l=1}^{NN} \Delta_l \psi_{il}[C_{dl} + (\phi_{\lambda l} - \theta_0)C_{ll}], \tag{6}$$

$$\sum_{j=1}^{N}\left[\delta_{ij}(\ddot{W}_j + \bar{\omega}_{wj}^2 W_j) + \mu D_{ij}\ddot{W}_j + E_{ij}\bar{W}_{\text{tip}} - \mu g\tau^2 E_{ij}/L + \beta\sum_{k=1}^{N} K_{jki}\Phi_j V_k\right]$$
$$= p\sum_{l=1}^{NN} \Delta_l \psi_{il}[C_{ll} - (\phi_{\lambda l} - \theta_0)C_{dl}], \tag{7}$$

$$\sum_{j=1}^{N}\left[\delta_{ij}(\bar{K}_m^2\ddot{\Phi}_j + \bar{K}_m^2\bar{\omega}_{\phi j}^2\Phi_j) + \beta\sum_{k=1}^{N} K_{ijk} V_j W_k + \beta\bar{W}_{\text{tip}} S_{ij} V_j\right]$$
$$= p\bar{c}\sum_{l=1}^{NN} \Delta_l \Theta_{il}\{C_{ml} - \bar{y}_{ac}[C_{ll} - (\phi_{\lambda l} - \theta_0)C_{dl})]\}. \tag{8}$$

The structural mode number is $i = 1, 2, \ldots, N$, and the aerodynamic section number along the span of wing is $l = 1, 2, \ldots, NN$. τ is a characteristic time scale, $\tau = \sqrt{mL^4/EI_1}$. $\bar{\omega}_{vj}, \bar{\omega}_{wj}$ and $\bar{\omega}_{\phi j}$ are jth nondimensional chordwise, vertical and torsional natural frequencies normalized by $1/\tau$. The time appearing in Eqs. (6)–(8) is also nondimensionalized by τ. $\bar{W}_{\text{tip}} \equiv W_{\text{tip}}/L$, is the nondimensional tip vertical displacement due to the manufactured curvature. μ is the nondimensional tip mass, $\mu = M/mL$. $\beta = EI_2/EI_1 - 1$ and $\lambda = \frac{1}{2}\rho U^2\bar{c}\tau^2/m$ are nondimensional stiffness and aeroelastic parameters. $K_{jki}, D_{ij}, S_{ij}, E_{ij}$ are coefficients depending upon the structural modes and manufactured curvature.

Eqs. (6)–(8) are the nonlinear equations of motion. A strictly linear flutter boundary is determined using Eqs. (6)–(8) by setting $\beta = 0$. For $\beta \equiv 0$, there is no effect on flutter of a pre-flutter static deflection or initial conditions. For $\beta \neq 0$ and a large static pre-flutter deformation, a dynamic perturbation approach is used to determine the small perturbation flutter boundary of this nonlinear system about a nonlinear and nontrivial static equilibrium condition.

Let $\{q\}$ be a state vector which is defined as

$$\{q\} = \{\dot{V}_j, V_j, \dot{W}_j, W_j, \dot{\Phi}, \Phi_j\}.$$

Using the perturbation approach, we define

$$q = \bar{q} + \hat{q} \quad \text{and} \quad \alpha_l = \bar{\alpha}_l + \hat{\alpha}_l, \tag{9}$$

where $\bar{q}$ and $\bar{\alpha}_l$ are the static equilibrium state variables and the corresponding quantities with a symbol of $\hat{(\ )}$ are the small dynamic perturbations about the static equilibrium state.

Substituting Eq. (9) into Eq. (6)–(8), a set of static equilibrium equations and dynamic perturbation equations is obtained. The static equilibrium equations comprise a set of nonlinear algebraic equations for the unknown state vector $\{\bar{q}\}$.

The dynamic perturbation equations about a static equilibrium state are

$$[\mathscr{A}]\{\dot{\hat{q}}\} + [\mathscr{B}]\{\hat{q}\} = \{0\}. \tag{10}$$

Note the coefficient matrices, $[\mathscr{A}]$, $[\mathscr{B}]$ are dependent on the flow velocity and the static equilibrium state, e.g. U, $\bar{q}$ and $\bar{\alpha}_l$, etc.

To determine the dynamic nonlinear response of this aeroelastic system, we can use Eqs. (6)–(8) and a time marching approach.

A note on the sign convention may be helpful here. Vertical bending deflection, w, and the direction of gravity are taken as positive up. Chordwise bending deflection, v, is taken as positive aft. And the torsional deflection and angle of attack are taken positive nose up. Note that since gravity is positive up, we are flying the wing upside down and, for example, a negative angle of attack is required to provide a lift downward to balance the wing weight.

Note that rigid-body motion has been neglected here since the primary purpose has been to study in support of subsequent wind tunnel studies of a cantilevered wing that have now been reported by Tang and Dowell (2002a,b).

3. Numerical results

Table 1 gives the structural and planform data for the cantilevered wing model under investigation, see Patil et al. (1999a). The wing structural modes retained in the analysis were two chordwise modes, five flap modes and two torsional modes. The wing is divided into 10 spanwise aerodynamic sections, i.e. $NN = 10$ and $\Delta_l = 0.1$. The static stall aerodynamic data used in this paper are as follows:

$$C_{ls} = \begin{cases} 2\pi \sin(\alpha/2\pi)\cos(\alpha/2\pi), & 0 \leqslant \alpha < 10^\circ, \\ 1.074 + 0.0052\alpha, & 10^\circ \leqslant \alpha < 15^\circ, \\ 1.1 - 0.0366\alpha, & 15^\circ \leqslant \alpha < 45^\circ, \\ 0.0, & \alpha > 45^\circ, \end{cases}$$

$$C_{ms} = \begin{cases} 0.0, & 0 \leqslant \alpha < 15^\circ, \\ -0.08, & 15^\circ \leqslant \alpha < 45^\circ, \end{cases}$$

$$C_{ds} = 1.7\alpha^2.$$

In the perturbation approach, ΔC_l is defined as

$$\Delta C_l = (\Delta C_l)_{\bar{\alpha}} + \left[\frac{\partial \Delta C_l}{\partial \alpha}\right]_{\bar{\alpha}} \hat{\alpha}.$$

For no static wing deformation, the strictly linear flutter speed and frequency corresponding to $\beta \equiv 0$ are found to be 32.5 m/s and 22.75 rad/s, respectively, close to the values determined by earlier investigators, see Patil et al. (1999a).

3.1. Perturbation eigenvalue solution

We use Eq. (10) to solve the perturbation eigenvalue problems for the following four cases.

3.1.1. Case with a tip mass (both tip mass inertia and gravity force are included)

A concentrated mass is added to the center of gravity at the tip of wing. Fig. 1(a) shows the first five structural natural frequencies vs the tip static displacement for a nondimensional tip mass, μ, ranging from 0 to 0.25. It is found that the vertical or flap natural frequencies decrease as μ increases or correspondingly the tip static displacement increases. The first torsional natural frequency greatly decreases and becomes zero at $\mu = 0.212$ corresponding to tip displacement of 1.62 m. Note the first chordwise natural frequency increases. These results are because of the significant nonlinear

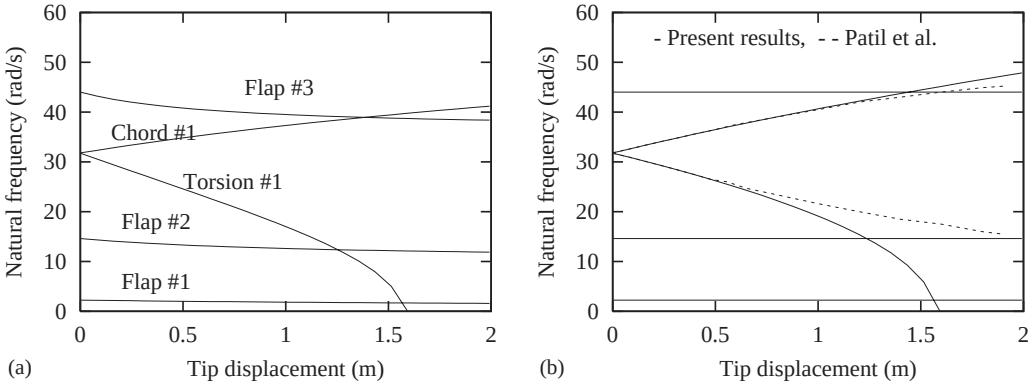

Fig. 1. Structural natural frequencies versus tip displacement (a) with tip mass [tip gravity force and tip mass inertia], and (b) tip gravity force only.

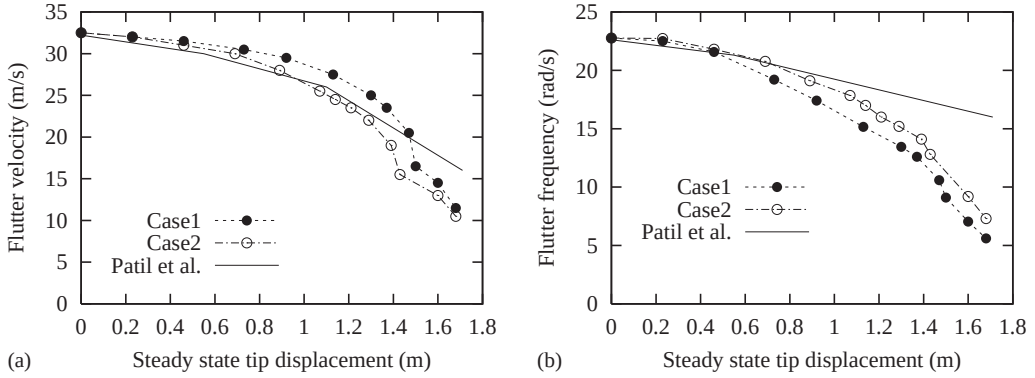

Fig. 2. Perturbation eigenvalue solutions of the linearized aeroelastic model versus steady state tip vertical displacement due to tip mass and tip force, giving (a) flutter velocity and (b) flutter frequency.

structural coupling between bending and torsion. Note also the first chordwise ($\omega_v = 31.74$ rad/s) and torsional ($\omega_\phi = 31.14$ rad/s) natural frequencies without a tip mass are almost equal which magnifies the nonlinear coupling effect.

The steady state tip vertical displacement is determined using the set of nonlinear static equilibrium equations and a Newton–Raphson solution method. The steady state tip vertical displacement increases monotonically as μ increases.

In Fig. 2, the flutter velocity and corresponding flutter frequency are shown to decrease with increasing steady state tip displacement (due to the tip mass).

3.1.2. Case with a tip force only (tip mass inertia is neglected)

The tip vertical load is the same as Case 1, but in this case we neglect the inertia of the tip mass. The natural frequency behavior due to the tip force is shown in Fig. 1(b) which is similar to Fig. 1(a). We find the first chordwise and torsional natural frequencies have the same behavior as in Fig. 1(a), but the vertical natural frequencies do not change when the tip mass inertia is neglected.

For comparison with earlier results from Patil et al. (1999a) for a tip force only, the latter data are also plotted in Fig. 1(b) as indicated by the dashed line. The results for the vertical frequencies are consistent with each other. The results for the coupled torsion/chordwise bending mode are very close for smaller steady state tip displacements, but significant differences are seen in the range of large tip displacement. This is not unexpected as the present analysis uses simpler equations which are restricted to smaller nonlinear responses compared to the structural model used in Patil et al. (1999a).

In Fig. 2, as indicated by the symbol, ◦, we again see that the flutter velocity and corresponding flutter frequency decrease with increasing steady state tip vertical displacement. Comparing the two results of Cases 1 and 2, it is concluded that the effect of the inertia force caused by the tip mass is small, but that the effect of the structural nonlinearity due to the tip gravity force is significant.

For comparison with earlier results from Patil et al. (1999a,b), the latter data are also plotted in Fig. 2 as indicated by the solid line. Corresponding to Fig. 1(b), and as expected, the present results and those of Patil et al. (1999b) are very close for the smaller steady state tip displacements, but more significant differences are seen in the range of large tip displacement.

3.1.3. Case with a manufactured curvature

The wing is assumed to have a manufactured curvature in the vertical direction. Its shape is expressed as follows:

$$w_0 = W_{\text{tip}}(\bar{x}^4 - 4\bar{x}^3 + 6\bar{x}^2)/3L.$$

This manufactured shape is close to the first vertical or flap bending natural mode. W_{tip} may be either positive or negative. In Fig. 3(a) the flutter velocity is shown and in (b) the flutter frequency. In this figure, the symbol, $\circ$, indicates the results obtained from plus W_{tip} and the symbol, $\triangle$, indicates the results obtained from minus W_{tip}. As expected the sign of W_{tip} (in the absence of gravity or a steady angle of attack) is unimportant and also qualitatively the results are similar to those for the two cases with a tip mass. This indifference to the sign of W_{tip} is physically intuitive and is also seen to follow from the analytical model.

3.1.4. Case for a steady angle of attack

When the steady angle of attack, θ_0, is not equal to zero, the static equilibrium position of the wing is significantly dependent upon the flow velocity. The consequent large initial vertical and torsional deformations affect the nonlinear flutter instability. Fig. 4 shows (a) the flutter velocity and (b) the flutter frequency. Note that again the results are indifferent to the sign of θ_0 in the absence of gravity. There are two kinds of instability found for the range of steady angle of attack shown. When $\theta_0 \leqslant 1^\circ$, there is a flutter instability, but the flutter velocity and oscillation frequency decrease as θ_0 increases. When $\theta_0 > 1^\circ$, there is a static divergence with zero oscillation frequency. The divergent velocity also decreases as θ_0 increases.

Comparing the above results with those of cases 1–3, the relationship between the steady state tip vertical displacement and the flutter velocity is shown for all four cases examined in this paper in Fig. 5. The numerical data for tip displacement in the figures are obtained just below the flutter or divergence velocity. As shown in Fig. 5, for the same steady state tip vertical displacement, the flutter velocity is lowest for the steady angle of attack case, highest for the tip force in the range of smaller tip vertical displacement and highest for the manufactured curvature in the range of larger tip vertical displacement. What is most significant however is the similarity of the results for all four cases. This is consistent with the earlier results of Patil et al. (1999a) who noted that there is a strong correlation of the flutter results with static tip displacement whatever the physical source of static deformation. This is easy to understand in that if the static deformation is the same whatever the physical mechanism for creating it, then the flutter condition will be the same. Of course, equal tip static displacement does not ensure the overall static deformation is the same, but it does suggest the static deformation patterns will be similar.

3.1.5. Case with wing mass gravity

When the wing mass gravity effect is included in Eqs. (1)–(3) and therefore in Eq. (10), we find the system is always divergent under any small flow velocity. This is because of the large initial static deformation in the vertical direction (the tip displacement is about 3 m). A parameter study has been made for several different wing masses and with other system parameters the same. The results are shown in Fig. 6 (a) for the flutter velocity and (b) corresponding flutter frequency versus the nondimensional wing mass. The solid line indicates the results with no wing mass gravity effect included and the symbol $\circ$ the results with the wing mass gravity effect included. In Fig. 6, the nondimensional wing mass is normalized by the original wing mass (0.75 kg/m). For the no-gravity case, the flutter velocity and frequency decrease as nondimensional wing mass increases due to decrease of the system natural frequencies. With gravity included, the flutter velocity and frequency greatly decrease as nondimensional wing mass increases and become 0 at 0.72 of the nominal wing mass.

3.1.6. Combined effects

First, we consider the combined effect of the wing mass gravity and a manufactured curvature. The manufactured curvature is opposite to the wing mass gravity direction. The results are shown in Fig. 7 for the divergent velocity vs the tip vertical displacement due to manufactured curvature. In the range less than 2.7 m and larger than 4.9 m for the tip displacement due to manufactured curvature, the system is divergent at very low flow velocity. In the range between 2.7 and 4.9 m, the divergent velocity decreases with increasing manufactured curvature from 15.5 to 12 m/s.

Second, we consider the combined effect of the wing mass gravity and a steady angle of attack. The steady angle of attack provides a steady lift to balance the wing mass gravity loading and therefore decreases the static wing

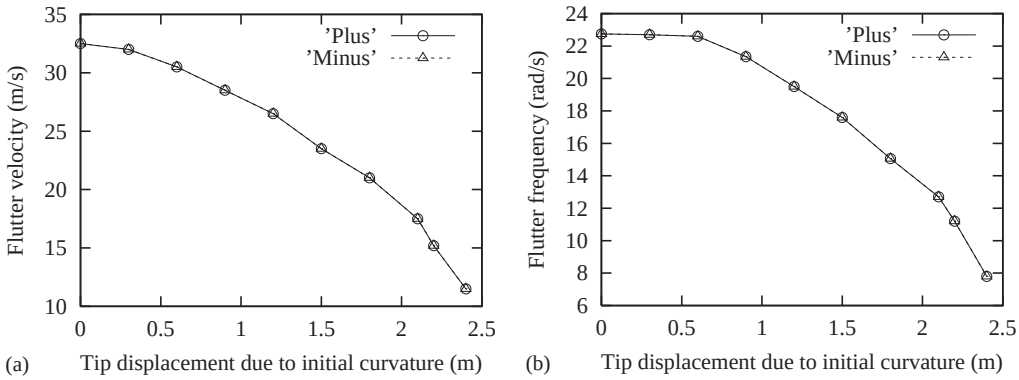

Fig. 3. Perturbation eigenvalue solutions of the linearized aeroelastic model vs steady state tip vertical displacement due to manufactured curvature, giving (a) flutter velocity and (b) flutter frequency.

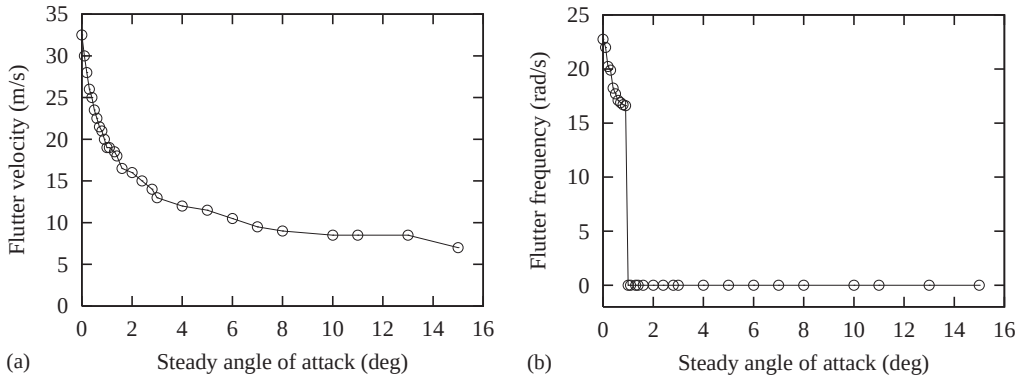

Fig. 4. Perturbation eigenvalue solutions of the linearized aeroelastic model vs steady angle of attack, giving (a) flutter velocity and (b) flutter frequency.

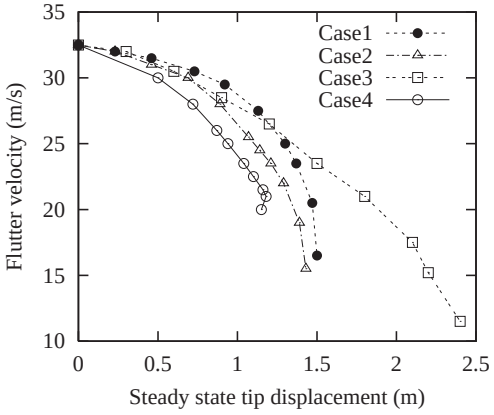

Fig. 5. Flutter velocity vs steady state tip vertical displacement due to tip mass, tip force, initial manufactured curvature and steady angle of attack.

deformation. Perturbation flutter velocities are calculated for a range of steady angle of attack. The results are shown in Fig. 8. Fig. 8(a) shows the perturbation flutter velocity vs steady angle of attack from $\theta_0 = -0.1^\circ$ to -4°. There are lower (denoted by the symbol ◦) and upper (denoted by the symbol •) flutter or divergent boundaries for a given steady angle of attack. For a flow velocity below the lower boundary, the system is unstable. The unstable behavior includes a

static divergence and a flutter instability. The flutter velocity of both the lower and upper unstable boundaries decreases with increasing steady angle of attack. For a flow velocity higher than the upper boundary, the system becomes unstable again. It is found the flutter velocity of the upper unstable boundary does not exceed the strictly linear flutter velocity (32.5 m/s) corresponding to $\beta \equiv 0$. Thus any static wing deformation leads to a decrease in system stability. In the flow velocity range between the lower and upper boundaries, the system is stable. The range of stable flow velocities is almost constant when $\theta_0 < -0.5^\circ$. This is because the system stable range corresponds to a certain range of the static deformation of the wing.

In Fig. 8(a), there is also shown a solid line between the lower and upper stability boundaries which corresponds to the total wing lift along the span equal to the total wing weight, i.e.,

$$\int_0^L \mathrm{d}F_w \, \mathrm{d}x = mgL.$$

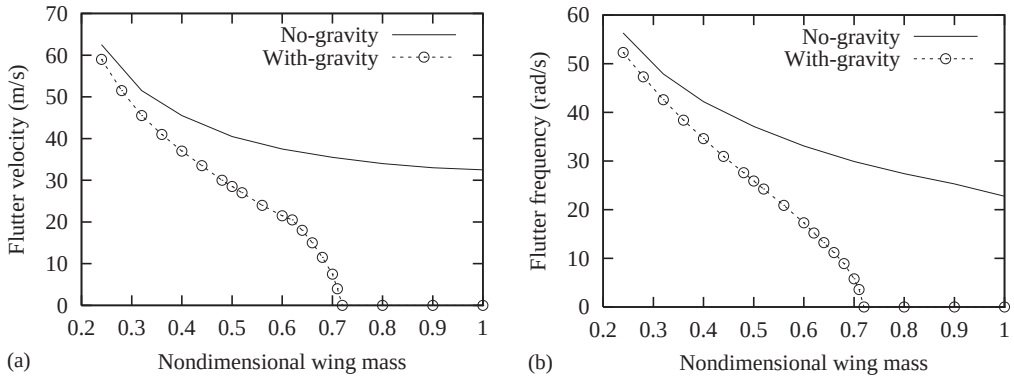

Fig. 6. Effects of wing mass gravity on perturbation eigenvalue solutions, giving (a) flutter velocity and (b) flutter frequency.

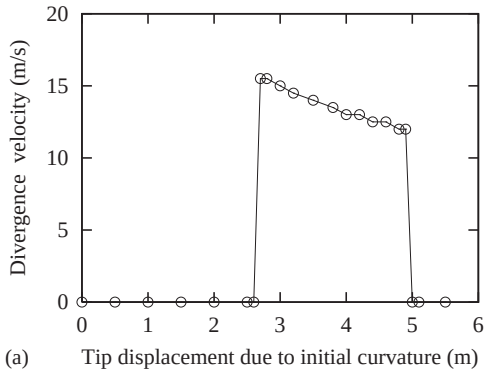

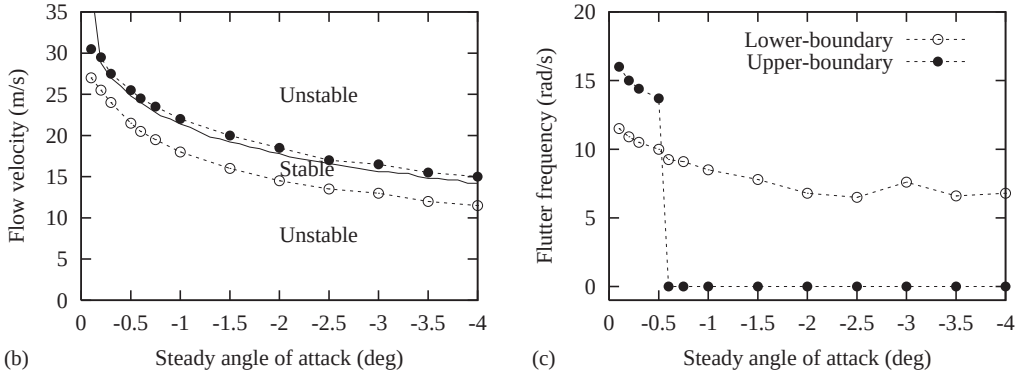

Fig. 7. Effects of combination between the wing mass gravity and manufactured curvature on the system stability.

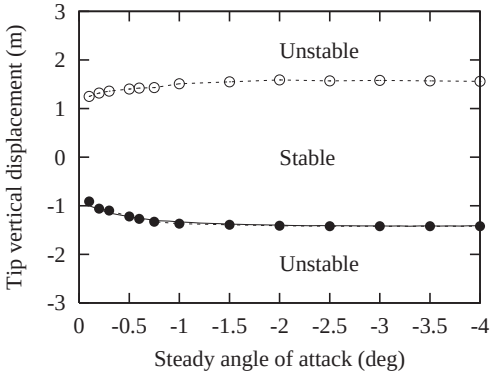

Fig. 8. Effects of combination of the wing mass gravity and a steady angle of attack on system stability: (a) flow velocity versus steady angle of attack; (b) flutter frequency versus steady angle of attack; and (c)tip vertical displacement vs steady angle of attack. [Note: With our sign convention these angles of attack are actually negative in sign.]

It is seen that this curve is close to the upper flutter boundary, but it does lie in the stable range. Thus for equilibrium in vertical flight the aircraft is stable. However disturbances to this equilibrium condition may easily lead to flutter.

Fig. 8(b) shows the flutter or divergence frequencies corresponding to Fig. 8(a). The flutter frequency of the lower unstable boundary decreases with increasing steady angle of attack. For the upper flutter boundary, the system becomes divergent when the steady angle of attack is less than -0.6°. Fig. 8(c) shows the corresponding tip vertical displacement vs the steady angle of attack. The upper tip displacement boundary as indicated by an open circle corresponds to the lower unstable flutter boundary and the lower tip displacement boundary as indicated by a closed circle corresponds to the upper unstable flutter boundary in Fig. 8(a). A solid line corresponding to lift equal to wing weight in Fig. 8(a) is also plotted in Fig. 8(c). This result is consistent with the tip displacement of the upper flutter boundary being close to that determined when the lift balances the wing weight.

3.2. Nonlinear time marching solution

3.2.1. Effect of initial conditions

We use Eqs. (6)–(8) for the nonlinear time marching solution. The purpose of these calculations is to find the effect of initial conditions on the flutter velocity and to determine any limit cycle oscillation when the flow velocity is above or below the flutter velocity. Fig. 9(a) shows flutter velocity vs. initial tip vertical displacement from 0.01 to 1.6 m for no manufactured curvature, and with a tip mass or tip force for $\mu = 0.05$. (The tip static vertical displacement is 0.6 m as measured from the static equilibrium state.) Also shown for reference is the case, $\mu = 0$ or no tip mass or force. Fig. 9(b) shows similar results for an initial twist angle. The initial condition is defined such that the initial wing deformation has (a) the first vertical mode shape or (b) first torsional mode shape. As shown in Fig. 9(a) the flutter velocity decreases with increasing initial tip vertical displacement for all three cases. The results for the tip mass and tip force are very close each other. As shown in Fig. 9(b) the results are similar to Fig. 9(a) for the no-mass case, but for cases 1 and 2 the initial tip twist does not affect the flutter velocity in the range lower than 5.5°.

3.2.2. Limit cycle oscillations

When we remove the nonlinear structural terms from Eqs. (6)–(8), but still include the ONERA model stall aerodynamic nonlinearities, an LCO response was found as shown in Fig. 10 for a flow velocity of $U = 33$ m/s. (Note the strictly linear flutter velocity is 32.5 m/s.) Fig. 10(a) shows the time history of the tip vertical response with a 0.1 m tip displacement initial condition and the corresponding FFT analysis is shown in Fig. 10(b). The motion includes two dominant frequency components. One is 22.8 rad/s which corresponds to the linear flutter frequency. The other is 44.7 rad/s which is close to the second harmonic of the flutter frequency and to the third vertical natural frequency. The response is dominated by the latter. Similar results are found for the chordwise and torsional responses. Fig. 11(a) shows the time history of the angle of attack at the tip and the corresponding FFT analysis is shown in Fig. 11(b). The angle of attack response also includes the same two frequency components as in Fig. 10, but now the dominant frequency component corresponds to the flutter frequency. The angle of attack is larger than the stall angle (it is $\alpha_s = 10^\circ$). When $U > 33.75$ m/s, it is found that the response becomes oscillatory divergent. From Figs. 10 and 11,

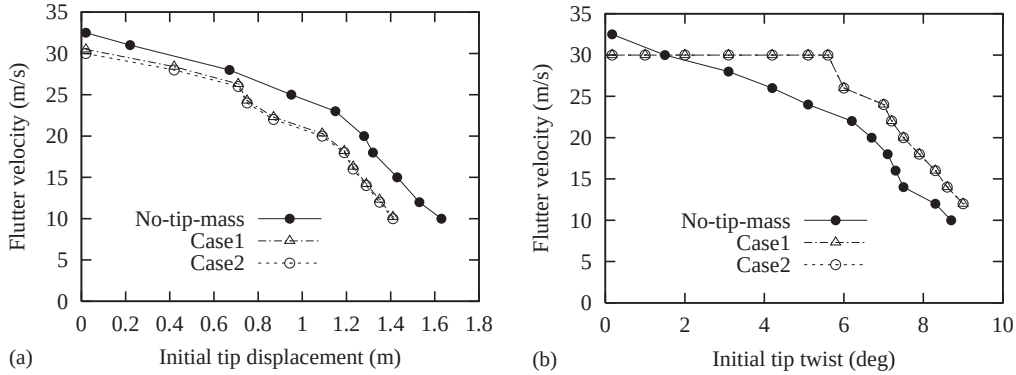

Fig. 9. Flutter velocity versus initial tip vertical displacement (a) and initial tip twist (b) for $\mu = 0$ and $\mu = 0.05$.

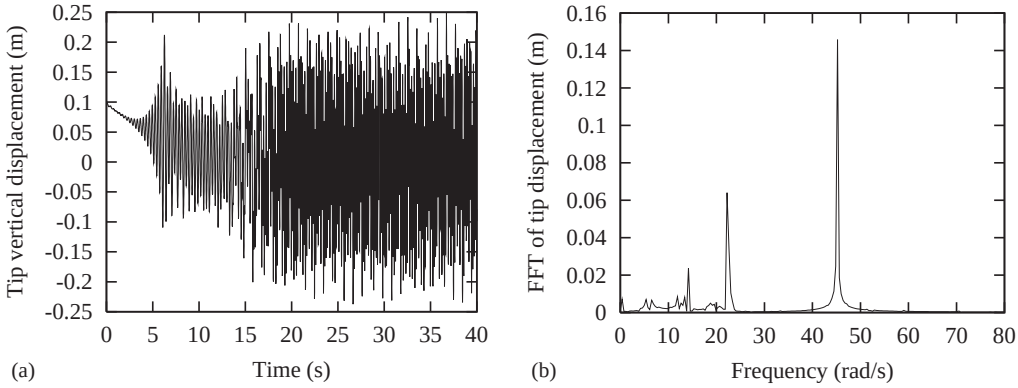

Fig. 10. (a) Time history and (b) corresponding FFT analysis of tip vertical response for linear structural system and $U = 33$ m/s.

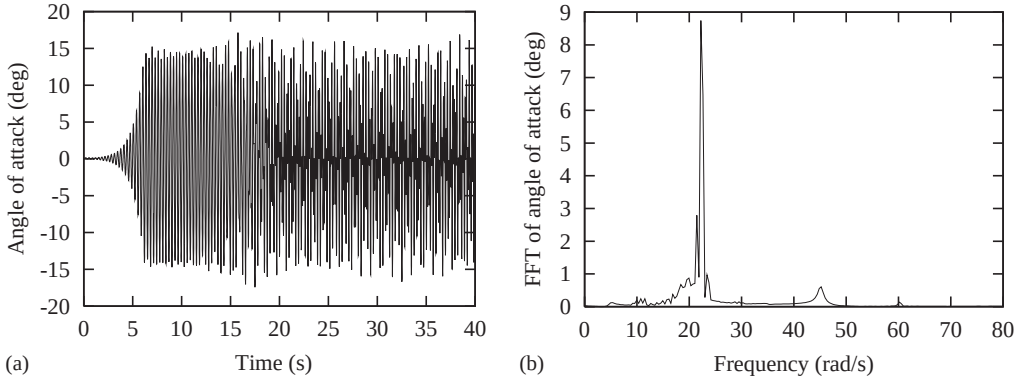

Fig. 11. (a) Time history and (b) corresponding FFT analysis of tip angle of attack for linear structural system and $U = 33$ m/s.

we conclude the stall aerodynamic nonlinearity leads to the limit cycle oscillation, and the LCO occurs over a relatively small range of flow velocity.

When the geometric structural nonlinearity is included in the equations, however, we did not find any LCO when the flow velocity is *larger* than the perturbation flutter velocity for either no initial steady state tip displacement or for a given initial steady state tip or torsional displacement. This is presumably because the structural nonlinear force decreases the system stiffness and hence stability. Although the static stall aerodynamics provide a mechanism for LCO above the perturbation flutter velocity, the effect of the structural nonlinearity overpowers the weaker aerodynamic

nonlinearity for the set of parameters investigated, and thus does not lead to a new steady state with a limit cycle oscillation for the present wing model.

For a given initial steady state tip or torsional displacement, we did find a LCO response when the flow velocity is *lower* than the perturbation flutter velocity. Figs. 12 shows the tip LCO amplitude (peak-to-peak) versus the flow velocity for the tip mass case of $\mu = 0.1$ and an initial tip displacement of 0.5 m. The perturbation flutter velocity is 29.5 m/s. When the flow velocities less than 23.8 m/s, no LCO is found. When the flow velocities lie between 23.8 and 24.3 m/s, the LCO is a periodic motion as indicated by ◦. A typical time history and corresponding FFT analysis are shown in Figs. 13(a) and (b) for $U = 24.1$ m/s. The peak-to-peak tip vertical displacement is 0.018 m and corresponding frequency is 12.56 rad/s.

When the flow velocities between 24.4 and 24.96 m/s, the LCO is a chaotic motion as indicated by a filled circle. The steady response becomes quite complex. A typical time history and corresponding FFT analysis are shown in Fig. 14(a) and (b) for $U = 24.5$ m/s. A phase plane plot is shown in Fig. 14(c). The steady response includes a high amplitude, low frequency oscillation and some higher frequency components with lower amplitude motions. The peak-to-peak LCO tip amplitude is about 0.12 m and corresponding FFT has a broader spectrum than the LCO at lower flow velocities.

When the flow velocities are higher than 24.974 m/s, the response becomes oscillatory divergent. A time history is shown in Fig. 15 for $U = 24.974$ m/s. It is noted that this velocity is well below the perturbation flutter velocity of about 29.5 m/s. This shows the dangerous effect of initial conditions or disturbances in inducing flutter or LCO.

More FFT analyses are shown in Figs. 16–18 for $U = 23.9$, 24.3, 24.4, 24.7 and 24.9 m/s. Note the LCO amplitudes shown in Figs. 12–18 are rather small and the LCO occurs over a relatively small range of flow velocity.

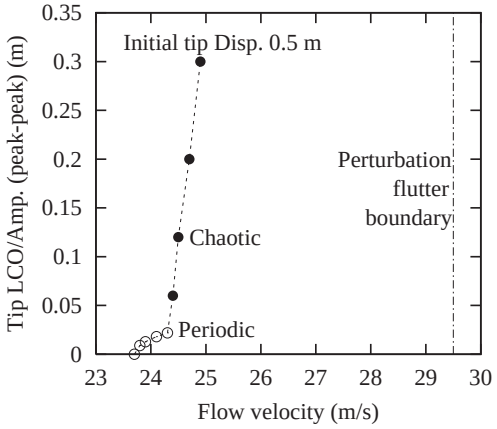

Fig. 12. Tip LCO amplitude (peak-to-peak) versus flow velocity for tip mass case of $\mu = 0.1$ and initial tip displacement 0.5 m.

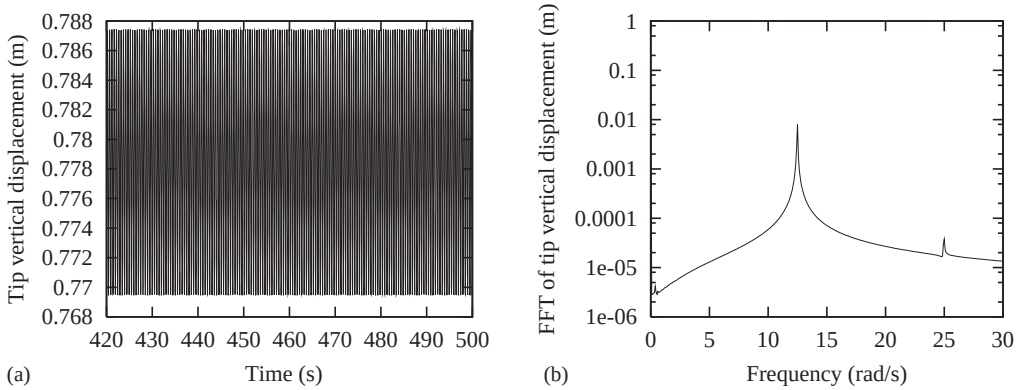

Fig. 13. (a) Time history and (b) corresponding FFT analysis of tip vertical displacement for $U = 24.1$ m/s.

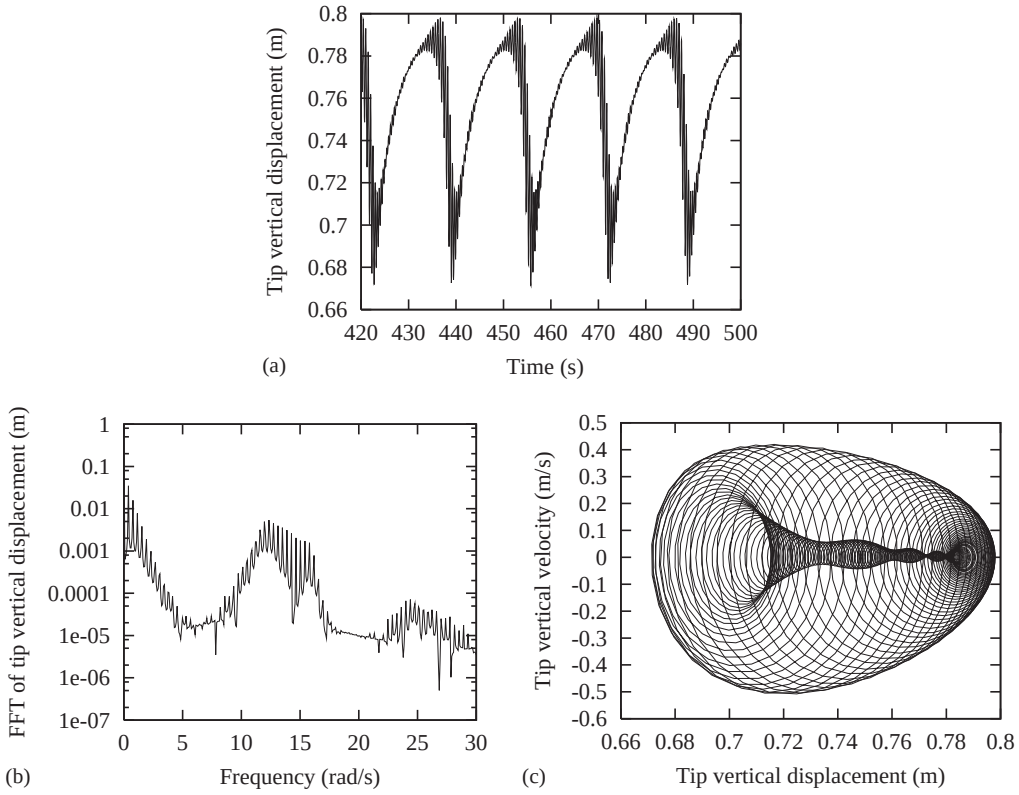

Fig. 14. (a) Time history and (b) corresponding FFT analysis of tip vertical displacement, and (c) phase plane plot for $U = 24.5$ m/s.

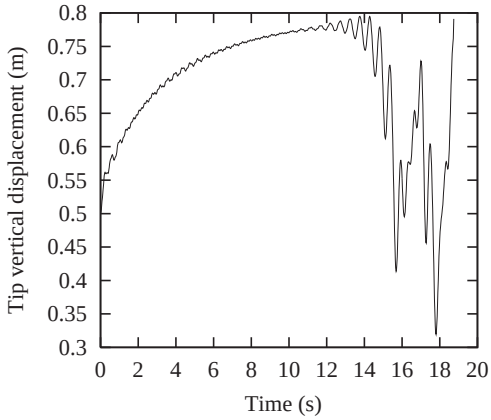

Fig. 15. Time history of tip vertical displacement for $U = 24.974$ m/s.

4. Concluding remarks

The present results are in agreement with those of earlier investigators notably Patil et al. (1999a,b). However they also provide new insights into the nuances of nonlinear aeroelastic phenomena for high-aspect-ratio wings that have a beam-like structural behavior. The effects of the geometric structural nonlinearity of the beam theory on both the flutter instability boundary and the nonlinear response are significant. In particular, the static deformation in the vertical or torsional directions caused by a static angle of attack, gravity and/or manufactured curvature generally decreases the

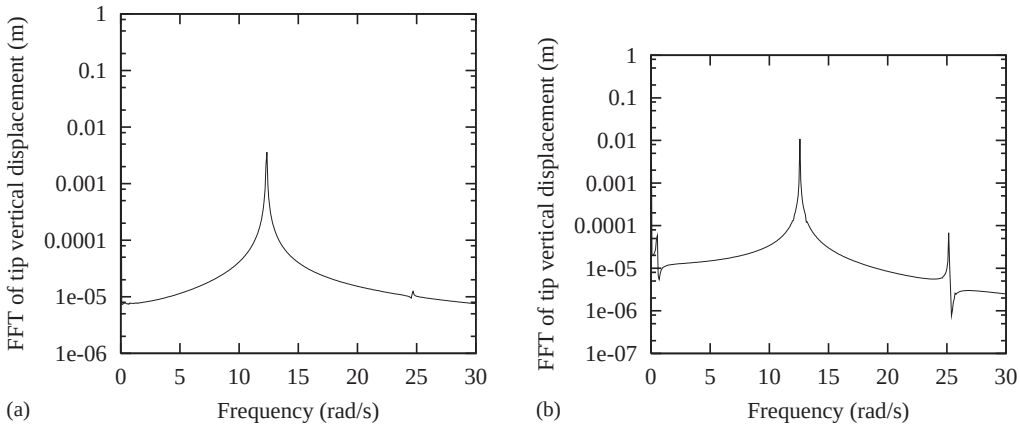

Fig. 16. The FFT analysis of tip vertical displacement for $U = 23.9$ m/s and $U = 24.3$ m/s.

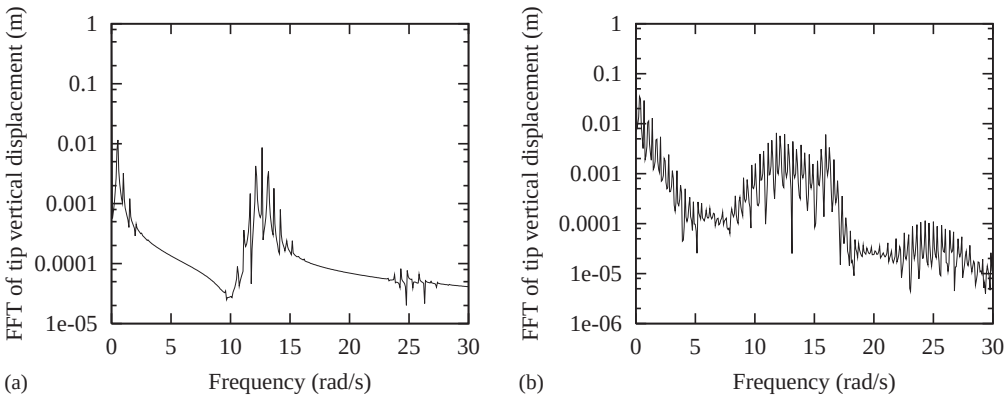

Fig. 17. The FFT analysis of tip vertical displacement for $U = 24.4$ m/s and $U = 24.7$ m/s.

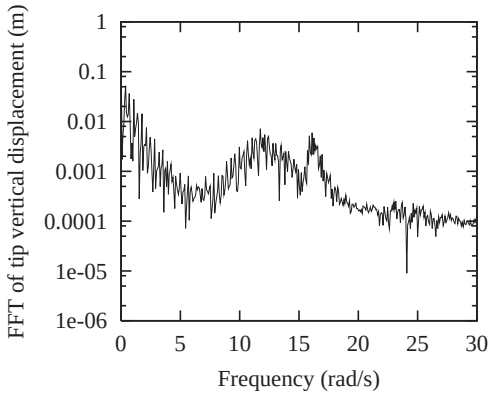

Fig. 18. The FFT analysis of tip vertical displacement for $U = 24.9$ m/s.

system stiffness and stability and also leads to a sensitivity to initial conditions and any parameter that influences the static equilibrium condition. The onset of a limit cycle oscillation is dependent upon a delicate balance between stall aerodynamics and structural nonlinear forces. LCO above and below the perturbation flutter boundary generally occurs over a limited range of flow velocity. LCO can occur below the perturbation flutter velocity due to large initial

disturbances. Finally, order of magnitude, analytical estimates have been developed for when structural nonlinearities may be important.

Acknowledgements

This work was supported under DARPA Grant, "Aeroelastic Leveraging and Control Through Adaptive Structures". Dr Ephrahim Garcia is the grant program officer. All numerical calculations were done on a supercomputer, T916, in the North Carolina Supercomputing Center (NCSC).

Appendix A. Order of magnitude estimates of the amplitudes of response when nonlinear effects become important

By comparing the relative size of the nonlinear and linear terms in the governing equations of motion, one can estimate the order of magnitude of the response when nonlinear effects become important. The calculations involve only simple algebra and some logic.

Dowell (1969,1970) has previously used these techniques to estimate the amplitude of the response of limit cycle oscillations of curved plates. Of course, a flat plate is a well known special case of the curved plate. Here we use the same technique to estimate the amplitude of response when nonlinear effects become important for the high aspect ratio wing model. In the present example of this paper, this technique will give an order of magnitude estimate of the static deflection required to change significantly the perturbation flutter velocity and the size of an initial condition required to change significantly this perturbation flutter velocity. It does not give us a good estimate for the LCO amplitude, however, because the LCO only occurs over a narrow range of flow velocity due to the destiffening and destabilizing effect of the softening structural nonlinearity which is dominant for this system.

It is interesting to note that Bejan (1983) has independently developed a methodology that he terms "scaling analysis" in the context of convection heat transfer models that is very similar to the approach of Dowell (1969,1970).

As an aside we briefly discuss the LCO amplitude arising from the aerodynamic stall nonlinearity, although this is a trivial case to make an order of magnitude estimate as to when nonlinear aerodynamic effects are important. As expected on physical grounds, the aerodynamic nonlinearity associated with the ONERA stall aerodynamic model becomes important when the angle of attack of the system response exceeds the stall angle in the ONERA model.

The structural nonlinearity is more subtle and interesting however. Consider the equations of structural motion as given in Eqs. (1–30) in the main text. To make our estimate as to when nonlinear effects become important we hypothesize this will occur when the nonlinear stiffness terms in these equations are comparable in size to the linear stiffness terms.

From Eq. (1), therefore, we require that on an order of magnitude basis

$$EI_2 v/L^4 \sim (EI_2 - EI_1)\phi w/L^4. \tag{A.1}$$

From Eq. (2) we require that

$$EI_1 w/L^4 \sim (EI_2 - EI_1)\phi v/L^4 \tag{A.2}$$

and from Eq. (3) we require that

$$GJ\phi/L^2 \sim (EI_2 - EI_1)wv/L^4. \tag{A.3}$$

From these three estimates we may solve for the following order of magnitude estimates:

$$v/w \sim \varepsilon^{1/2}, \tag{A.4}$$

$$\phi \sim \varepsilon^{1/2}(1-\varepsilon)^{-1}, \tag{A.5}$$

$$w/L = (GJ/EI_2)^{1/2}(1-\varepsilon)^{-1} \tag{A.6}$$

and

$$\varepsilon \equiv EI_1/EI_2. \tag{A.7}$$

Note that, typically, $\varepsilon \ll 1$, and (A.5), (A.6) may be correspondingly simplified. But if $\varepsilon \to 1$, the system becomes linear and (A.5) and (A.6) correspondingly predict that there is no finite amplitude for which nonlinear effects will be detected.

Using the data for GJ, EI_1 and EI_2 from Table 1 in the main text we determine the following estimates for the response levels for v, w and ϕ for which nonlinear effects become important:

$$w/L \sim \left(\frac{1\times 10^4}{4\times 10^6}\right)^{1/2} = 1/20.$$

$$\Rightarrow w \sim 0.7\ \text{m};$$

$$\phi \sim \left(\frac{2\times 10^4}{4\times 10^6}\right)^{1/2} \sim (200)^{-1/2} \sim 4^\circ.$$

Recalling Fig. 1, we see that the estimate for w is comparable to that magnitude of the static tip displacement at which significant changes in system natural frequencies are seen and from Fig. 2 we see this is also the response magnitude when significant changes in the flutter velocity and frequency are seen. Also see Fig. 5, for example. These order of magnitude estimates are also consistent with the initial conditions or disturbances for w or ϕ required to induce a measurable reduction in the flutter speed from its small perturbation value, see Fig. 9. These estimates are not as useful for the LCO per se, since the LCO occurs over a narrow velocity range and the LCO amplitude of response starts at zero and over a short range of velocity moves off to infinity when the LCO itself becomes dynamically unstable, see Fig. 12. One could claim an agreement in the range of finite LCO response with these order of magnitude estimates, but clearly these estimates are not particularly useful when the LCO occurs over a limited range of a parameter such as flow velocity. On the other hand, these estimates are reliable guides to when nonlinear effects become important due to a pre-flutter static deformation and/or because of finite initial conditions and disturbances for the present system. When the LCO occurs over an extended parameter range as in Dowell (1969,1970), these estimates are useful for determining the LCO response as well.

Thus this method of making order of magnitude estimates is useful, but it does require some physical insight into the behavior of the system and some numerical data to help interpret the meaning of these estimates.

References

Bejan, A., 1984. Convection Heat Transfer. Wiley, New York.

Dowell, E.H., 1969. Nonlinear flutter of curved plates. AIAA Journal 7, 424–431.

Dowell, E.H., 1970. Nonlinear flutter of curved plates, Part II. AIAA Journal 8, 259–261.

Hodges, D.H., Dowell, E.H., 1974. Nonlinear equations of motion for the elastic bending and torsion of twisted nonuniform rotor blades. NASA TN D-7818.

Patil, M.J., Hodges, D.H., Cesnik, C.E.S., 1999a. Limit cycle oscillations in high-aspect-ratio wings. AIAA Paper-99-1464.

Patil, M.J., Hodges, D.H., Cesnik, C.E.S., 1999b. Nonlinear aeroelasticity and flight dynamics of high-altitude long-endurance aircraft. AIAA Paper-99-1470.

Tang, D.M., Dowell, E.H., 2002a. Experimental and theoretical study of gust response for a high-aspect ratio wing. AIAA Journal 40, 419–429.

Tang, D.M., Dowell, E.H., 2002b. Limit cycle hysteresis response for a high-aspect ratio wing model. Journal of Aircraft 39, 885–888.

Tang, D.M., Dowell, E.H., Hall, K.C., 1999a. Limit cycle oscillations of a cantilevered wing in low subsonic flow. AIAA Journal 37, 364–371.

Tang, D.M., Henry, J.K., Dowell, E.H., 1999b. Limit cycle oscillations of delta wing models in low subsonic flow. AIAA Journal 37, 1355–1362.

Tran, C.T., Petot, D., 1981. Semi-empirical model for the dynamic stall of airfoils in view to the application to the calculation of responses of a helicopter blade in forward flight. Vertica 5, 35–53.